AD_____

Award Number: DAMD17-99-1-9391

TITLE: Assessment of the Viscoelastic Properties of Normal and Abnormal Breast Tissue

PRINCIPAL INVESTIGATOR: Donald B. Plewes, Ph.D.

CONTRACTING ORGANIZATION: Sunnbrook & Women's College
Health Sciences Centre
Toronto, Ontario M4N 3M5 Canada

REPORT DATE: July 2001

TYPE OF REPORT: Annual

PREPARED FOR: U.S. Army Medical Research and Materiel Command
Fort Detrick, Maryland 21702-5012

REPORT DOCUMENTATION PAGE

Form Approved
OMB No. 074-0188

1. AGENCY USE ONLY (Leave blank)	2. REPORT DATE	3. REPORT TYPE AND DATES COVERED
	July 2001	Annual (1 Jul 00 - 30 Jun 01)

4. Assessment of the Viscoelastic Properties of Normal and Abnormal Breast Tissue

5. FUNDING NUMBERS
DAMD17-99-1-9391

6. AUTHOR(S)
Donald B. Plewes, Ph.D.

7. PERFORMING ORGANIZATION NAME(S) AND ADDRESS(ES)
Sunnbrook & Women's College
Health Sciences Centre
Toronto, Ontario M4N 3M5 Canada
E-Mail: don.plewes@swchsc.on.ca

8. PERFORMING ORGANIZATION REPORT NUMBER

9. SPONSORING / MONITORING AGENCY NAME(S) AND ADDRESS(ES)
U.S. Army Medical Research and Materiel Command
Fort Detrick, Maryland 21702-5012

10. SPONSORING / MONITORING AGENCY REPORT NUMBER

11. SUPPLEMENTARY NOTES

12a. DISTRIBUTION / AVAILABILITY STATEMENT
Approved for Public Release; Distribution Unlimited

12b. DISTRIBUTION CODE

13. Abstract ***(Maximum 200 Words)*** *(abstract should contain no proprietary or confidential information)*

It is well known that variations in biomechanical properties of breast tissue are associated with the presence of disease. As a result, it is thought that stiffness represent an attractive property by which to detect disease and aid in differentiation between normal and benign breast tissues. Over the past few years, a number of investigators have attempted to measure breast tissue biomechanical properties based on ex-vivo tissue samples. These studies suggest the presence of large variations in breast tissue elastic modulus among various breast tissues. These data, however, are subject to sampling errors arising from tissue heterogeneity within the tissue samples and potential differences arising from ex-vivo conditions and tissue sample handling. As a result, repeatable measurements have been hard to achieve and the obtained data are thus less reliable. Our goal in this project is to study these properties with an MRI method, both in-vitro and in-vivo, and assess the biomechanical properties of fat, fibroglandular and cancerous breast tissues. During our first year of funding, we have initiated the development of two uniaxial loading systems, an MRI-based and table-top system. Also, we developed various inverse solution algorithms for reconstruction of elastic modulus using MRI derived displacement data. During our second year, we have integrated, optimized and tested the table-top system. Using animal tissues, this system has proven to be accurate and reliable, and we are in the process of starting measurements on breast tissues. In addition, we have developed and optimized a novel constrained elastography technique which will be used in in-vivo breast tissue modulus measurement.

14. SUBJECT TERMS	15. NUMBER OF PAGES
Biomechanis, MRI, Elastography, Finite Element Method Breast Cancer	24
	16. PRICE CODE

17. SECURITY CLASSIFICATION OF REPORT	18. SECURITY CLASSIFICATION OF THIS PAGE	19. SECURITY CLASSIFICATION OF ABSTRACT	20. LIMITATION OF ABSTRACT
Unclassified	Unclassified	Unclassified	Unlimited

Table of Contents

MRI Assessment of the Viscoelastic Properties of Normal and Abnormal Breast Tissue: Annual Report to the US Army

INTRODUCTION

It is well known that variations in tissue elasticity properties are associated with the presence of cancer. Data from the literature[1,2] suggest that by measuring the elastic properties of tumors and lesions compared to normal breast tissue, the relationship between pathological processes and elasticity can be investigated. During the past several years, a number of researchers[3,4,5,6,7] have been attempting to use MRI elastography to assess the biomechanical properties of breast tissue. The subject of this research project is to obtain a better understanding of the biomechanical properties of breast tissue by accurately measuring their stiffness both in-vivo via MRI elastography and invitro using a precision loading system. The results of this investigation have the potential of aiding in improved diagnosis of breast cancer and predicting tissue deformation. The latter is very important in various medical applications such image coregistration.

Our approach to measure the biomechanical properties of breast tissues will be to apply MRI motion detection methods to measure tissue strain while the surface is undergoing external forces with an applicator. By an analysis of the resulting motions and through the use of an appropriate elasticity reconstruction technique, we aim to measure the distribution of tissue elastic properties in-vitro and in-vivo. These measurements will be performed on a number of normal breast tissue samples and a number of breast tissue pathologies will be obtained from pathology. Based on these data, the feasibility of determining the type of breast tissue abnormality and predicting tissue deformation in-vivo will be assessed.

RESEARCH TASK – Year II

This project is a three-year project with a number of separate research goals and tasks. During the second year, three tasks were to be performed as follow:

Task I - The first task is to test, integrate and optimize our precision table-top loading system for in-vitro elasticity measurement of breast tissues.

Task II - For MRI based elasticity measurement, the second task was to develop a modulus reconstruction algorithm which inputs the MRI derived displacement data of the sample undergoing quasi-static loading and outputs the relative elastic moduli of different tissue components within the sample.

Task III - An important application of this research is predicting breast tissue deformation. Beside the fact that this model is used in our modulus reconstruction algorithm, it can be applied in many other medical applications such as breast image coregistration. In parallel to the second task, the third task was to develop a Finite Element (FE) model that requires the biomechanical properties of breast tissues to predict tissue deformation. This model has been successfully used as the forward model

component of our reconstruction technique as well as to demonstrate other potential medical applications of this project such as breast image coregistration.

PROGRESS TO DATE

Task I - Precision table-top system

During the first year, we started the design and configuration of a table-top uniaxial system to measure tissue elastic properties in-vitro. Throughout the second year, this system has been tested, modified and integrated to provide both accurate measurements as well as conditions similar to those of in-vivo. This system is shown in ***Figure 1*** and it allows for table-top uniaxial loading experiments under a broad range of frequencies and amplitudes. This system consists of two main components: a linear stepper motor actuator used to deform the tissue sample in a programmable fashion and a load cell for force measurement. The applied tissue deformation is measured based on the motion delivered by the actuator, while measuring the resulting force dynamically with the load cell. The actuator and load cell are wired to a computer that gives instructions to the actuator and receives data from both the actuator and the load cell through Labview virtual instrument software. To provide conditions similar to those of in-vivo, tissue samples are kept moist by immersing them in an isotonic sodium chloride solution, and temperature is maintained at 37°c using a temperature control device. This temperature control device is yet to be tested with biological tissues. The loading system has been tested with chicken breast tissue. Five samples were prepared and their Young's modulus measured. As a result, the mean value and standard deviation of these measurements were 5.3 Kpa and 0.4 kPa respectively which suggests that the system provides both accurate and repeatable measurements.

Task II - Constrained Modulus Reconstruction Technique

During the first year of this project, an MR compatible loading system was designed and configured which allows controlled compression of small tissue samples and phantoms for testing purposes. In addition, Navier equations based moduli reconstruction algorithms were developed to be used in conjunction with the loading system. To achieve a reasonable reconstruction results, however, very high SNR values are required which are very difficult to obtain in practice. As an alternative, we have developed an iterative constrained modulus reconstruction technique with moderate SNR requirement. This technique has been tested on a multi-component phantom with a 3-D complex geometry and the results indicate that the reconstruction algorithm is reasonably accurate and robust. ***Figure 2*** depicts the phantom's geometry and the modulus reconstruction results obtained from this technique. A manuscript outlining the mathematics and results of this technique has been submitted for publication and is now in press in *IEEE-Transactions on Medical Imaging.* To apply this technique for in-vivo breast tissue modulus reconstruction, a breast compression system shown in ***Figure 3*** has been designed and constructed. This system consists of two compression plates, one stationary and the other is driven by the MR compatible stepper motor to compress the breast sinusoidally. At this stage, this system is being tested on a breast shaped phantom shown in ***Figure 4.*** This figure shows a sagittal MR image of this phantom with a preliminary coronal strain image of the phantom. Although encouraging, the strain image suggests that further improvement to the compression system is required to achieve better SNR.

Task III – Breast Tissue Deformation Model

Modeling breast tissue deformation is a very important task for this research project as it is the primary component of our constrained elasticity reconstruction technique. For this reason, in parallel to the modulus reconstruction technique, we have developed 3-D FE model that uses breast MRI images and tissue mechanical properties as an input and calculates tissue deformation and stress distribution as an output. This model is capable of predicting both small deformation as in the case of breast elastography as well as large deformation as required in other applications such as image coregistration. This, however, requires the hyperelastic properties of the breast tissues to be known. The details of this model and its application in breast image coregistrationis presented in a paper[8] which was published recently in *IEEE-Transactions on Medical Imaging.*

FUTURE WORK

The research that was originally proposed for this project remains valid. Conclusions from the first and second years' research suggest that it is feasible to utilize MRI imaging to measure breast tissue biomechanical properties. This concept has been proven using experimental data with a phantom and simulated data with a volunteer's breast as presented in our modulus reconstruction paper[8]. After testing the temperature control system mounted on our table-top uniaxial loading system, we will start measurements of breast tissue elastic modulus in-vitro. In the mean time, after improving our breast compression, we will conduct in-vivo breast elastography experiments in conjunction with our modulus reconstruction algorithm. In addition, we will attempt to measure breast hyperelastic properties in-vitro which are very important in predicting breast tissue large deformation.

KEY RESEARCH ACCOMPLISHMENTS

1) The construction of a precision table-top loading system to perform in-vitro breast tissue elasticity measurement. This system has been tested and proven to be relatively accurate and reliable. In-vitro breast tissue elasticity measurement will be started in the near future.

2) The development of a constrained modulus reconstruction technique for in-vivo breast elastography using MRI derived displacement data. A paper outlining this technique will be published shortly in *IEEE-Transactions on Medical Imaging.* This paper suggests that very moderate SNR values are required for reasonably accurate modulus reconstruction. In addition, a breast compression device has been constructed and tested with a breast shaped phantom. The preliminary results of this test is encouraging, however, further improvement is required to achieve better SNR values required for in-vivo experiments.

3) The development of a breast tissue deformation model using MRI data has been completed and a paper outlining the mathematics and method has been published recently in *IEEE-Transactions on Medical Imaging*[8]. This model is capable of predicting the displacements and stress distribution of breast tissues while undergoing both small and large deformation.

REPORTABLE OUTCOMES

During the past year, we have submitted a number of papers and symposium abstracts, as detailed below, which relate to the research contained in this project.

PUBLISHED OR SUBMITTED MANUSCRIPTS:

1) Samani A, Bishop J, Yaffe MJ and Plewes DB. Biomechanical 3-D finite Element Modeling of the Human Breast Using MRI Data. IEEE Transactions on Medical Imaging 20(4):271-279, 2001.

2) Samani A, Bishop J and Plewes DB. A Constrained Modulus Reconstruction Technique for Breast Cancer Assessmant. IEEE Transactions on Medical Imaging, 2001 (in press).

3) Bishop J, Samani A, Sciarretta J, Luginbhul C and Plewes DB. A Signal/Noise Analysis of Quasi-static MR Elastography. Submitted to IEEE Transactions on Medical Imaging, 2001

ABSTRACTS:

1) Samani A, Bishop J and Plewes D. A Constrained Breast Magnetic Resonance Elastography Technique: 3D Phantom Study. International Society for Magnetic Resonance in Medicine: Nineth Annual Meeting, Glasgow, April 21-27, 2001, Paper#1640.

2) Samani A, Bishop J and Plewes D. 3D Finite Element Model for Breast Non-rigid Registration. International Society for Magnetic Resonance in Medicine: Nineth Annual Meeting, Glasgow, April 21-27, 2001, Paper#837.

3) Bishop A, Samani A and Plewes D. A Signal/Noise Analysis of Magnetic Resonance Strain Imaging. International Society for Magnetic Resonance in Medicine: Nineth Annual Meeting, Glasgow, April 21-27, 2001, Paper#1646.

CONCLUSIONS

During the first and second years of this project, we have made good progress toward our end goal of understanding the biomechanical properties of breast tissues and developing the means to apply these in tissue deformation analyses. The overall objective of this project was to create reliable mathematical tools to predict tissue deformation in the presence of compression to determine tissue properties of various breast tissues, both normal as well as benign and neoplastic tissues. We have, thus far, been able to develop the hardware and software tools required to conduct this study. In addition, we have used these tools with phantoms and animal tissues and the results indicate that they are reasonably accurate and reliable. During the third year of this project, we will use these tools to measure the biomechanical properties of breast tissues using samples we will obtain from pathology. The importance of this work remains high providing a platform for new detection and diagnosis methods for breast cancer. This work can also open up new applications of breast imaging including data fusion and therapy planning tools based on predictive tissue deformation analysis

capabilities such as the breast tissue deformation model we developed in the second year of this project.

REFERENCES

1. Sarvazyan A, Goukassian D, Mavesky E and Oranskaja G. Elasticity Imaging as a New Modality of Medical Imaging for Cancer Detection. Proceeding of International Workshop on Interaction of Ultrasound with Biological Media, Valenciennes, France, 5-9 April 1994, pp 69-81.

2. Krouskop TA, Wheeler TM, Kallel F, Garra BS and Hall T. Elastic Moduli of Breast and Prostate Tissue Under Compression. Ultrasonic Imaging 20, 260-274, 1998.

3. Plewes DB, Betty I, Urchuk S and Soutar I. Visualizing Tissue Compliance with MR. Journal of Magnetic Resonance Imaging 5(6):733-738, 1995.

4. Bishop JB, Poole G, Leitch M and Plewes DB. Magnetic Resonance Imaging of Shear Wave Propagation in Excised Tissue. Journal of Magnetic Resonance in Medicine 8:1257-1265, 1998.

5. Chenevert T, Skovoroda A, O'Donnell M and Emelianov S. Elasticity Reconstruction Imaging by Means of Stimulated Echo MRI. Magnetic Resonance in Medicine 39: 482-490, 1998.

6. Muthupillai R, Lomas D, Rossman P, Greenleaf J, Manduca A and Ehman R. Magnetic Resonance Elastography by Direct Visualization of Propagation Strain Waves. Science 26: 1854-1857, 1995.

7. Sinkus R, Lorenzen J, Schrader D, Morenzen M, Dargatz M and Holz D. High-Resolution Tensor MR Elastography for Breast Tumour Detection. Physics in Medicine and Biology 45:1649-1664, 2000.

8. Plewes DB, Bishop J, Samani A and Sciarretta J. Visualization and Quantization of Breast Cancer Biomechanical Properties with Magnetic Resonance Elastography. Physics in Medicine and Biology 45(6):1591-1610, 2000.

Appendix 1: Figures of the body of the proposal

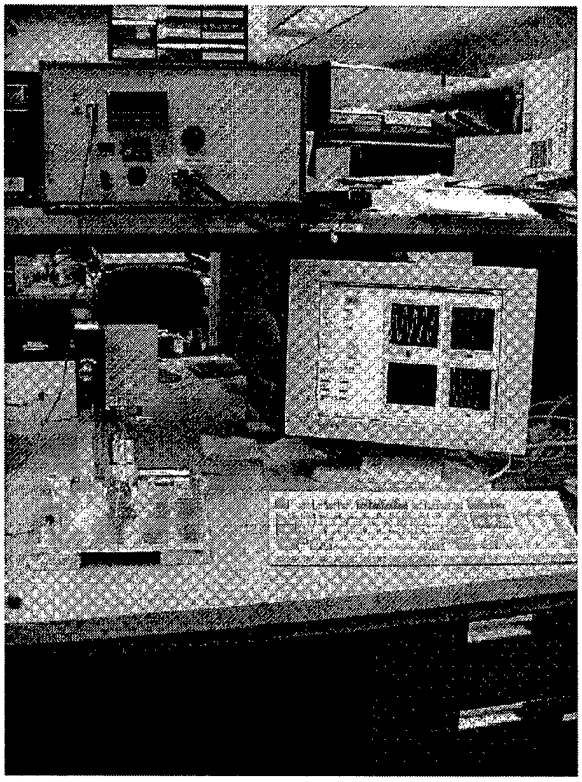

Figure 1. Precision table-top uniaxial loading system for in-vitro tissue measurement. This system consists of two main component: a linear stepper motor actuator used to deform the tissue sample in a programmable fashion and a load cell for force measurement.

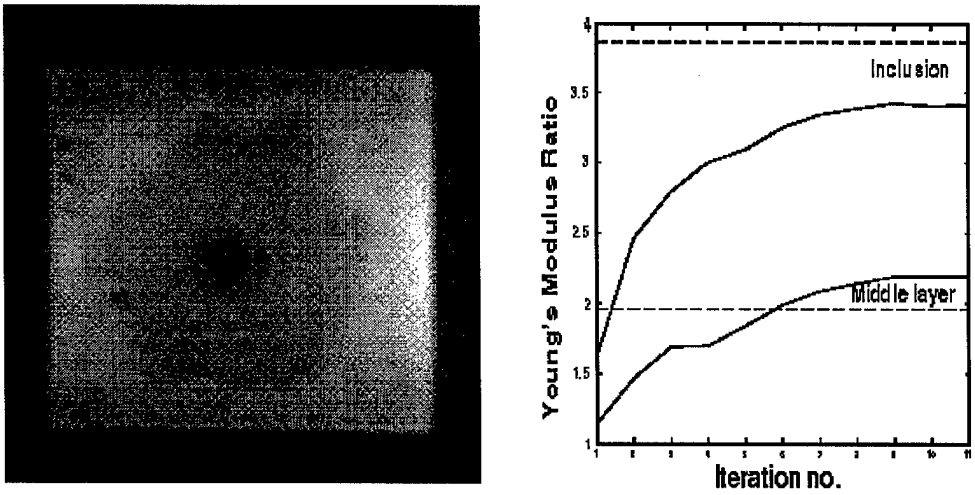

Figure 2. MRI image of the multi-layer phantom (left) and reconstruction results using the constrained reconstruction technique (right). The reconstruction results indicate a maximum error of 12% in reconstructing the modulus of different layers

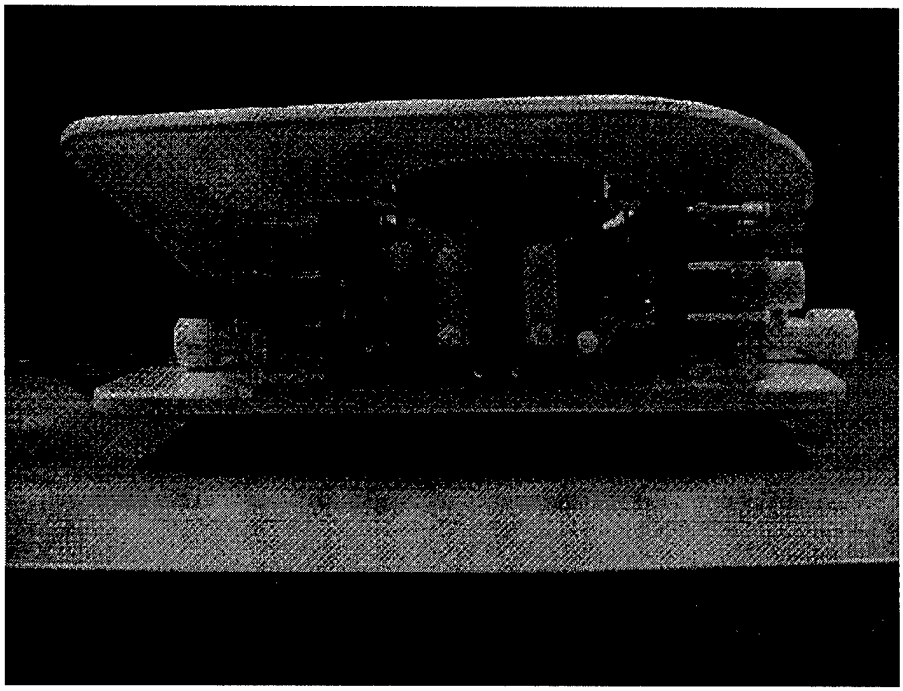

Figure 3. MRI compatible breast compression system used for MR elastography of a breast-shaped phantom. This system consists of commercial breast coil and an assembly of plates and cams which deliver sinusoidal compression to the breast via an MR compatible stepper motor.

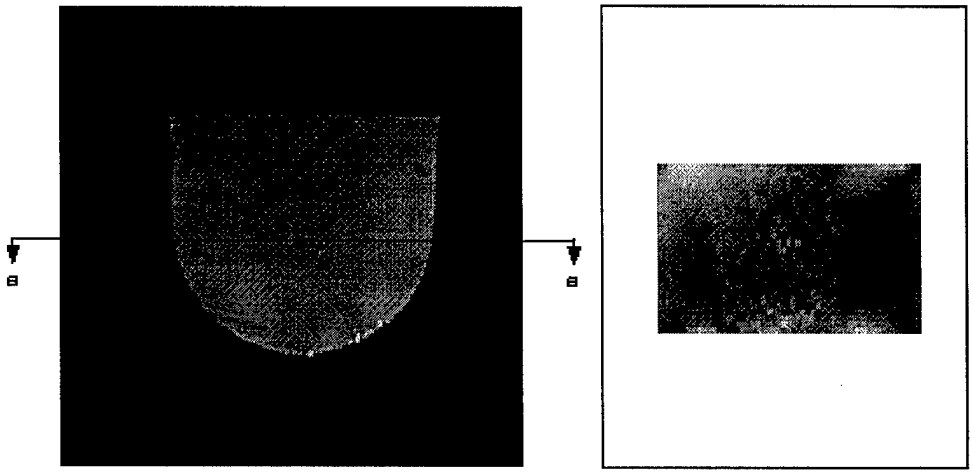

Figure 4. MRI sagittal image of the breast-shaped phantom (left) and a strain image a coronal slice corresponding to section a-a (right). Although the strain SNR is not satisfactory, different layers of the phantom are visible.

Appendix 2: Published abstracts and papers

Abstracts:

1) Samani A, Bishop J and Plewes D. A Constrained Breast Magnetic Resonance Elastography Technique: 3D Phantom Study. International Society for Magnetic Resonance in Medicine: Nineth Annual Meeting, Glasgow, April 21-27, 2001, Paper#1640.

2) Samani A, Bishop J and Plewes D. 3D Finite Element Model for Breast Non-rigid Registration. International Society for Magnetic Resonance in Medicine: Nineth Annual Meeting, Glasgow, April 21-27, 2001, Paper#837.

3) Bishop A, Samani A and Plewes D. A Signal/Noise Analysis of Magnetic Resonance Strain Imaging. International Society for Magnetic Resonance in Medicine: Nineth Annual Meeting, Glasgow, April 21-27, 2001, Paper#1646.

A Constrained Breast Magnetic Resonance Elastography Technique: 3D Phantom Study

A. Samani, J. Bishop, and D. B. Plewes
Department of Medical Biophysics, University of Toronto

Introduction Tissue elasticity, defined by Young's modulus, is well known to be associated with the presence of cancer. Compared to normal fibroglandular tissue, recent studies [1] suggested a 6 fold increase in the Young's modulus of breast carcenoma while fibroadenomas are only a factor of 3 stiffer. These observations indicate that an imaging modality which is based on elasticity contrast can improve specificity. This have stimulated the development of breast MR elastography (MRE) techniques [2,3] with the aim of imaging tissue Young's modulus. In these techniques, harmonic [2] or quasi-static [3] motion is mechanically induced within the tissue, the resulting tissue deformation is measured by MRI techniques, from which the tissues' Young's modulus distribution can be calculated via an inversion technique. In [3], we presented a quasi-static MRE technique which proved to be successful based on a simple 2d phantom study, and a breast study using simulated data. In this article, we present the results of a 3d phantom consisting of three different layers with complex geometry to simulate adipose, fibroglandular and tumour tissues. Also, for breast MRE, modulus reconstruction results using an efficient finite element (FE) technique is presented.

Methods This technique is similar to the iterative reconstruction MRE technique presented in [3] where the geometry of each tissue type is assumed to be known *apriori*. Quasi-static sinusoidal compression of 0-5 mm amplitude is applied at the surface of the phantom using a MR compatible device and the resulting deformation is measured using a stimulated echo (STEAM) pulse sequence. The iterative modulus reconstruction process consists of tissue stress calculation using the FE method followed by modulus updating of each element using Hooke's law. At each iteration, the modulus of each tissue type is calculated by averaging over its corresponding volume. For breast MRE, we used a transfinite interpolation (TI) technique [4] which is based on the idea of mapping a unit square to any given enclosed region. This technique can model the breast's curved surface more efficiently than the previously used voxel based meshing technique. Moreover, this technique is capable of using variable FE size which makes it possible to increase the number of elements involved in averaging in the tumour, if necessary.

Results A cubic plastisol PVC phantom composed of a a 12 mm spherical stiff volume representing a tumour surrounded by a softer volume representing fibroglandular tissue was constructed. The latter was enclosed by another softer third layer representing adipose tissue. The Young's moduli of the individual layers were measured independently using a uniaxial benchtop experiment, resulting in 48.0 kPa, 24.3 kPa and 12.4 kPa for the three layers. MRI images of this phantom was acquired using a 3d fast spin-echo sequence with TR/TE=2000/85 ms and 48 echos. The phantom was placed in the compression device where it underwent a quasi-static sinusoidal compression of 3.5 mm amplitude. A STEAM pulse sequence with TR/TE=660/12 ms and a mixing time T_m of 300 ms was used to acquire displacement data in the central plane shown in Figure 1. Starting with Young's modulus ratios obtained from the measured strain image as an initial guess, as shown in Figure 1, convergence was achieved after 11 iterations. The final reconstructed modulus ratios indicate that there is a maximum error of 12%. For breast MRE, we used a volunteer's breast MRI image to create a 3d FE mesh using the TI based method. A sagittal slice of this mesh, where a simulated tumour is added, is depicted in Figure 2.

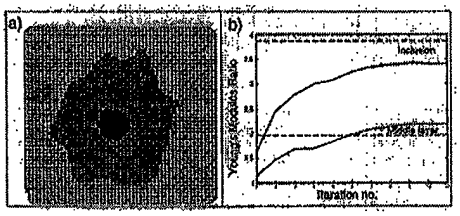

Figure 1: a) FE mesh of the phantom's central plane and b) reconstructed modulus ratios where the dashed lines represent the measured modulus ratios.

The Young's modulus of the adipose, fibroglanular, tumour and skin tissues were assumed to be 2.0 kPa, 10.0 kPa, 50.0 kPa and 25.0 kPa respectively. Accordingly, displacements resulting from 5 mm compression normal to the sagittal plane were calculated using a contact problem FE model. The displacement component in the compression direction was contaminated by normally distributed noise to simulate SNR value of 10. Using this displacement component and starting with modulus ratios obtained from the strain image, as shown in Figure 2, convergence to the true values was achieved after 7 iterations.

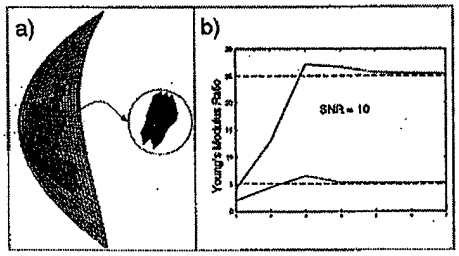

Figure 2: a) FE mesh of a breast slice b) MRE results where the dashed lines represent the exact modulus ratios.

Conclusions This article presents new developments in our previous constrained breast MRE technique [3]. This technique is very efficient as it requires imaging only one displacement component in one slice. Using a phantom consisting of 3 layers with complex 3D geometry, it was shown that this technique is capable of solving the breast MRE problem where the 3D stress and strain calculation as well as image segmentation are challenging. Furthermore, to improve the performance of our technique, we used a TI based FE meshing technique which leads to better geometry representation and allows using variable element size in the FE mesh. The latter, as demonstrated in the breast MRE example, can lead to a larger number of elements in the tumour to suppress the noise effects through averaging while the FE problem size does not change significantly.

References

[1] Wellman P. S. "Tactile Imaging". PhD thesis, Harvard Uni., 1999.
[2] Sinkus R. *et al. Phys. Med. Biol.* 2000; 45:1649–1664.
[3] Samani A. *et al.* 8th Annual Meeting of ISMRM 2000.
[4] Knupp P. and Steinberg S., "Fundamentals of grid generation", 1994.

3D Finite Eelement Model for Breast MRI Non-rigid Registration

A. Samani, J. Bishop, and D. B. Plewes
Department of Medical Biophysics, University of Toronto

Introduction Various medical applications often require comparison or data fusion of MR images that are acquired at different times. For example, to determine a breast tumour growth over time, radiologists need to compare the latest MR image with MR images acquired previously. However, since it is inevitable that MR images are acquired under different breast compressions or body positions, tissues will deform and, thus, lead to significant changes in the anatomical geometry. As such, image registration is required to facilitate image comparison or data fusion. Many researchers such as [1] have used voxel-based similarity measure concepts in their registration algorithms ignoring the physics behind tissue deformation. Based on an alternate methodology, in this article, we present a non-rigid image registration model for the breast based on biomechanics. We use a 3D nonlinear Finite Element (FE) model as a numerical solution to solve the breast tissue deformation problem.

Methods and Theory We use a 3D FE model based on the finite deformation theory of elasticity in conjunction with hyperelastic material to model large deformations of the breast undergoing medical procedures. In a static condition, the equilibrium equation of an object under applied forces is:

$$\frac{\partial \sigma_{i1}}{\partial x_1} + \frac{\partial \sigma_{i2}}{\partial x_2} + \frac{\partial \sigma_{i3}}{\partial x_3} + f_i = 0; \qquad i = 1,2,3 \qquad (1)$$

where the σ's denote the Cauchy (true) stress tensor components and f_i represents the body forces. Assuming that a strain energy function U is selected as a function of the strain invariants $\bar{I}_1$, $\bar{I}_2$ and J, σ can be obtained from [2]:

$$\sigma = \frac{2}{J}\left[\left(\frac{\partial U}{\partial \bar{I}_1} + \bar{I}_1 \frac{\partial U}{\partial \bar{I}_2}\right)\bar{\mathbf{B}} - \frac{\partial U}{\partial \bar{I}_2}\bar{\mathbf{B}}.\bar{\mathbf{B}}\right] + \frac{\partial U}{\partial J}\mathbf{I} \qquad (2)$$

where $\bar{B}$ is a function of the deformation gradient and I is the identity matrix. We use ABAQUS: a commercial FE software [2] which solves equations (1) and (2) numerically to calculate the displacements. For FE mesh generation using hexahedral elements, MR images are first segmented using AnalyzeAVW 2.5 to detect breast edges and separate fat and fibroglandular tissues. The segmented images are, thus, processed using a transfinite interpolation meshing technique as described in [3]. Assuming that the displacement boundary conditions are known, the breast tissue displacement field can be calculated. This displacement field in conjunction with the MR image of the breast acquired prior to the movement is used to calculate an MR image consistent with the new configuration.

Results The mesh generation technique was first validated using a 60×60×60 mm cubic phantom made of agar with a hard cylindrical inclusion. MR image of the phantom was acquired and a FE mesh was created after image segmentation. Another FE mesh was created manually based on the phantom's known geometry. Using these meshes, a lateral compression of 9.0 mm was simulated with ABAQUS and the corresponding displacements were calculated at the inclusion's interface where maximum error is expected. As a result, the average difference between these displacements was less than 0.5% For breast image nonrigid registration, T_1 weighted sagittal MR images of a healthy volunteer, a typical image of which is shown in Figure 2a, were acquired with a GE SIGNA 1.5 T scanner. We used a 2-D spin-echo pulse sequence with $TR/TE = 300/9$ ms and $\theta = 90°$. The objective here was to calculate MR images of this breast as if it underwent 8.0 mm lateral compression by two rigid plates. For this purpose, a FE mesh was created and the compression was simulated using a 3D contact problem model. A FE mesh of a typical slice and a schematic of the contact problem model are depicted in Figure 1. For the fat and fibroglandular tissues, Neo-Hookean hyperelastic models were calculated using Wellman 1999 data [4] while the skin was assumed to be elastic with a Young's modulus of 25.0 kPa.

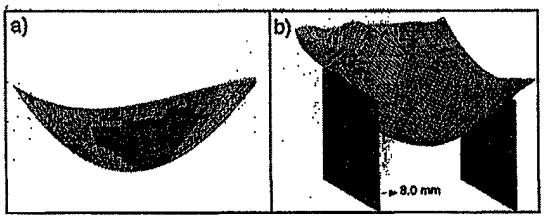

Figure 1: a) FE mesh of a sagittal slice and b) contact problem model of the breast.

Using ABAQUS, the problem was solved and the displacements were calculated. These displacements, in conjunction with the precompression MR image, were used to calculate the post compression MR image. A sagittal image and its corresponding calculated post compression image are shown in Figure 2.

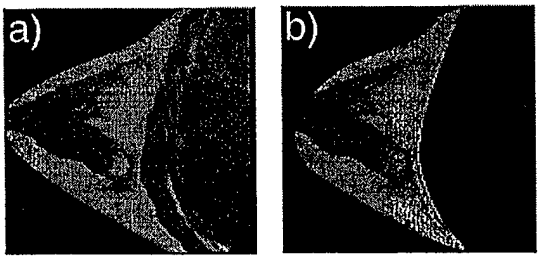

Figure 2: a) Precompression MR image and b) calculated post compression image of the breast.

Conclusions This article presents a biomechanics based 3D FE model which can be used for breast image nonrigid registration. This model is based on the finite deformation theory of elasticity. For mesh generation, we used a meshing technique we have developed using the transfinite interpolation method. This technique was validated and found to be accurate for displacement calculation. Breast tissues were modeled using hyperelastic Neo-Hookean models while the skin was assumed to be elastic. The results shown in Figure 2, qualitatively, prove the merits of this model. However, further research is required to test the model quantitatively.

References

[1] Rueckert *et al. IEEE Trans. on Med. Im.* 1999; 18:712-721.
[2] Hibbit *et al.* "ABAQUS, Theory Manual", 1998.
[3] Samani A. *et al. IEEE Trans. on Med. Im.*, in press.
[4] Wellman P. S. "Tactile Imaging". PhD thesis, Harvard Uni., 1999.

A Signal/Noise Analysis of Magnetic Resonance Strain Imaging

J. Bishop, A. Samani and D.B. Plewes
Department of Medical Biophysics, University of Toronto, Toronto, Ontario, Canada

Introduction In MR elastography, images of displacement within tissue or a phantom are obtained during a repeatable deformation. We and others have used stimulated-echo phase-contrast MR imaging[1,2,3] to obtain the displacement data. Strain, which is the spatial gradient of displacement, represents a simple but effective means of displaying the results of MR elastography because it is easy to compute and relatively straightforward to interpret. In this abstract, we extend the analysis of Steele et al[4] by describing and validating an analytic expression for strain/noise ratio. The expression is applicable to stimulated echo methods and can be used to design an elastography experiment for maximum strain SNR.

Theory Assume that a uniform object is compressed from the top surface in the vertical (y) direction and is fixed at the bottom surface. If the pulse sequence of figure 1 is used to measure the y displacement by phase-contrast, then the phase signal within the object Θ will be proportional to vertical displacement u as a function of height y:

$$\Theta(y) = 2\pi\Phi_d u(y), \qquad \Theta(0) = u(0) \equiv 0 \qquad (1)$$

where $\Phi d=\gamma G\tau$ is the zeroth moment of the displacement encoding gradient pulse. If L is the height of the object, then the strain is given by the average phase gradient is:

$$\frac{\partial\Theta}{\partial y} \cong \frac{\Theta(L)}{L} = \frac{\theta}{h} \qquad (2)$$

where θ is the average phase dispersion per pixel, and h is the size of a pixel.

The well-known relation for phase noise per pixel is

$$\sigma = \frac{1}{\sqrt{2}SNR} \qquad (3)$$

where SNR is the signal/noise of the magnitude data. In computing the discrete phase gradient of (2) by a central difference approximation, the phase noise becomes:

$$\sigma = \frac{1}{\sqrt{2}h}\frac{1}{\sqrt{2}SNR} \qquad (4)$$

where h is the pixel size from (2). The ratio of (2) and (4) can then be interpreted directly as the strain/noise ratio:

$$SNR_{strain} = 2SNR\theta, \quad \theta < \pi \qquad (5)$$

If $\theta > \pi$, the imaging point-spread function eliminates all signal[5]. Finally, the magnitude SNR term in (5) is expanded by explicitly writing the magnitude signal attenuation caused by the diffusion sensitivity of the displacement encoding pulses:

$$SNR_{strain} = 2SNR\, e^{-\phi_d^2(\tau-\frac{\tau}{3})D}\theta, \quad \theta < \pi \qquad (6)$$

where D is the apparent diffusion coefficient.

Methods Imaging experiments were conducted with quasi-static compression and a stimulated echo pulse sequence (Figure 1) gated to the compression cycle. A uniform cubic phantom of dimension 25 mm, made of 1% agar, was compressed by 1 mm at a frequency of 2 Hz. Imaging time was adjusted to achieve a base SNR (ie with no displacement encoding) in the magnitude data of about 30. Data were collected for a range of displacement-encoding sensitivities at constant echo time. Mean strain and strain noise were measured from experimental data and compared to the predictions of (6).

Results Figure 2 plots the theory (——) and experimental results for both the magnitude (o) and strain (+) SNR. The encoding sensitivity is plotted on the x-axis, expressed in terms of the phase dispersion per pixel θ. Note that θ and encoding sensitivity Φd are related through the surface displacement u(L) in (1) and (2). The SNR of the magnitude data drops off sharply as θ increases, due to diffusion sensitivity. Although the diffusion coefficient was not independently measured, a value of $D=2.05\times10^{-9}$ m^2/s fits the data well.

As expected the strain SNR (+) initially increases with increasing amount of phase dispersion θ. The strain SNR goes through a maximum value, then quickly drops off to zero well before the theoretical maximum encoding of π radians per pixel can be achieved, indicating that the experiment is limited by diffusion sensitivity. The predicted strain SNR from (6) is shown by the solid line, with good agreement to experiment.

Conclusions We have derived and validated a simple expression for strain SNR in quasi-static MR elastography using stimulated echoes. The presentation separates the diffusion sensitivity from all other terms contributing to magnitude SNR, and simplifies the experimental process of choosing the encoding sensitivity. For small surface displacements, the diffusion sensitivity of the encoding pulses clearly limits the achievable strain SNR. Although stimulated echoes are preferable for static and quasi-static methods where velocities are small, spin-echoes can be used to reduce diffusion sensitivity at the possible expense of increased T2 sensitivity in longer echo times.

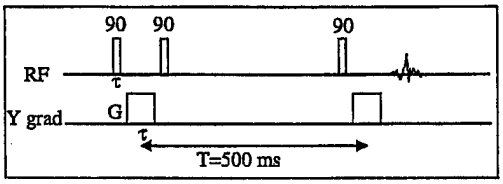

Figure 1: STEAM sequence used for strain imaging

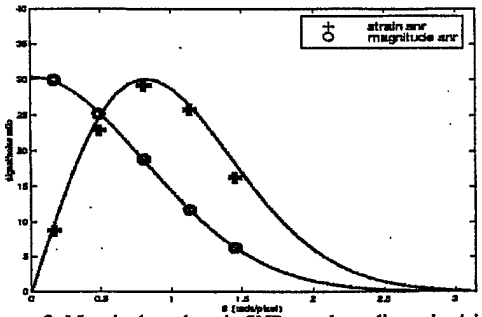

Figure 2: Magnitude and strain SNR vs. phase dispersion/pixel

References
[1] T.L. Chenevert *et al.* MRI. MRM 39:482-490 (1998).
[2] D.B. Plewes *et al.* PMB 45:1591-1610 (2000).
[3] A.H. Aletras *et al.* JMR 140, 41-57 (1999).
[4] D.D. Steele *et al.* Proc ISMRM 1999, pg 1616.
[5] VJ Wedeen *et al.* MRM 32:116-120 (1994

Paper:

Samani A, Bishop J, Yaffe MJ and Plewes DB. Biomechanical 3-D finite Element Modeling of the Human Breast Using MRI Data. IEEE Transactions on Medical Imaging 20(4):271-279, 2001.

Biomechanical 3-D Finite Element Modeling of the Human Breast Using MRI Data

Abbas Samani*, Jonathan Bishop, Martin J. Yaffe, and Donald B. Plewes

Abstract—**Breast tissue deformation modeling has recently gained considerable interest in various medical applications. A biomechanical model of the breast is presented using a finite element (FE) formulation. Emphasis is given to the modeling of breast tissue deformation which takes place in breast imaging procedures. The first step in implementing the FE modeling (FEM) procedure is mesh generation. For objects with irregular and complex geometries such as the breast, this step is one of the most difficult and tedious tasks. For FE mesh generation, two automated methods are presented which process MRI breast images to create a patient-specific mesh. The main components of the breast are adipose, fibroglandular and skin tissues. For modeling the adipose and fibroglandular tissues, we used eight noded hexahedral elements with hyperelastic properties, while for the skin, we chose four noded hyperelastic membrane elements. For model validation, an MR image of an agarose phantom was acquired and corresponding FE meshes were created. Based on assigned elasticity parameters, a numerical experiment was performed using the FE meshes, and good results were obtained. The model was also applied to a breast image registration problem of a volunteer's breast. Although qualitatively reasonable, further work is required to validate the results quantitatively.**

Index Terms—**Breast, finite element analysis, image registration, mesh generation, MRI.**

I. Introduction

PREDICTING breast tissue deformation is of great significance in several medical applications such as surgery, biopsy and imaging. In breast surgery, surgeons are often concerned with a specific portion of the breast, e.g., tumor, which must be located accurately beforehand. Locating the portion of interest is done using imaging techniques which are done under tissue configuration of compression or body position that is often entirely different from that of surgery. In this case, nonrigid image registration is required to locate the portion of interest in the new configuration. In breast biopsy, the biopsy needle causes the breast tissue to deform which may lead the tumor to displace. This deformation renders the guiding images less accurate unless the displacements are determined and needle aiming is corrected accordingly. In multimodality imaging of the breast, images of different modalities are often obtained under different tissue configurations of compression, orientation, or body position. In this case, determining the tissue deformation is essential for facilitating data fusion [1]. FEM has been widely used in modeling biological tissues such as bone [2]–[4] and myocardium [5], and recently in modeling brain deformation [6]–[8]. This work is aimed at using FEM in modeling breast tissue deformation.

For a FE model to be satisfactory in predicting deformation and other relevant parameters, in addition to using accurate elasticity parameters and boundary conditions, a reasonably accurate FE geometry model is essential. As the breast is composed of soft tissues, large deformation is usually created while undergoing medical procedures. In this paper, large deformation is considered in the FE formulation, and soft tissues are modeled as incompressible hyperelastic materials based on the experimental data of [9]. Viscoelastic response is not taken into account in this model as we do not expect it to be important on the short time scales, such as in breast medical applications. Nevertheless, it is possible to incorporate viscoelasticity into our model provided that relevant parameters are available. Boundary conditions in medical applications are usually displacement type which are known relatively accurately. In multimodality imaging which involves X-ray mammography, the boundary conditions are not fully known as the contact surface cannot be identified easily. However, a contact problem formulation as presented in [1] can be used which only requires the magnitude of the compression plate movement.

For breast FE mesh generation, marching-cubes-based techniques such as [10] can be implemented. However, the tetrahedral elements used in these techniques are well known to have unfavorable characteristics, such as slow convergence with mesh refinement. Also, these elements may exhibit overstiffening and volumetric locking especially with incompressible material [11], [12]. Accordingly, with biological soft tissues which are known to be incompressible, using hexahedral elements in the FE model is cost effective and more accurate. To our knowledge, there has been no work done for patient-specific mesh generation of the breast using hexahedral elements. However, computed tomography (CT) has been used by a number of investigators to automate mesh generation in bone. Many investigators [2], [13]–[17] have applied edge-detection algorithms on CT images to generate boundary contours of the struc-

Manuscript received August 9, 2000; revised December 6, 2000. This work was supported by the Terry Fox Foundation under Program Project Grant 006886 and by the U.S. Army under Grant DAMD 17-99-19391. The Associate Editor responsible for coordinating the rewiew of this paper and recommending its publication was M. W. Vannier. *Asterisk indicates corresponding author.*

*A. Samani is with the Department of Medical Biophysics, Imaging/Bioengineering Research Group, Sunnybrook and Women's College Health Sciences Centre, University of Toronto, 2075 Bayview Ave., Toronto, ON, M4N 3M5, Canada (e-mail: asamani@sten.sunnybrook.utoronto.ca).

J. Bishop was with the Department of Medical Biophysics, Imaging/Bioengineering Research Group, Sunnybrook and Women's College Health Sciences Centre, University of Toronto, Toronto, ON, M4N 3M5, Canada. He is now with Colorado MEDtec, Inc., Boulder, CO 80301 USA.

M. J. Yaffe and D. B. Plewes are with the Department of Medical Biophysics, Imaging/Bioengineering Research Group, Sunnybrook and Women's College Health Sciences Centre, University of Toronto, Toronto, ON, M4N 3M5, Canada.

Publisher Item Identifier S 0278-0062(01)02773-2.

tures in each image, then employed some techniques to generate the internal mesh. This strategy often requires a significant investment of time by an expert user, and is incapable of automatically generating reasonably accurate meshes for heterogeneous and geometrically complex objects. Other investigators [18]–[20] developed techniques that directly convert image voxels to eight noded hexahedral elements. The resulting object surfaces in these techniques are characterized by abrupt transitions and right angles. As a result, FEM leads to less accurate results, especially on the surface [21], [22]. This paper presents two methods for generating three-dimensional (3-D) meshes of the breast using magnetic resonance imaging (MRI) data. The first method converts image voxels to hexahedral elements and is similar to the said methods except that edge detection is done semi-automatically via segmentation. The second method is based on the transfinite interpolation (TI) technique [23] which is more accurate and efficient in creating smooth surfaces.

To validate the mesh generation component of this model, a cubic agarose phantom with a cylindrical inclusion was constructed and imaged using MRI. Using these images, FE meshes were created using the meshing techniques presented in this paper. To assess the accuracy of these methods, another mesh was created manually based on the known geometry of the phantom. The FEM was applied to these meshes to calculate the deformation and stress distribution resulting from a lateral compression similar to X-ray mammography procedures. The results obtained from both meshes compare well with the manually created mesh results except for the inclusion's circular interface where, as expected, the TI-based mesh produced better results. To demonstrate a potential clinical application of this model, MR images of a healthy volunteer's breast was acquired and a FE mesh was created using the meshing techniques. A lateral compression similar to X-ray mammography procedures was simulated using the TI-based mesh, and calculated MR images are presented in the postcompression configuration.

II. Methods

A. Governing Equations

We use a 3-D FE model to predict breast tissue deformation based on the biomechanical parameters of the breast tissues. While undergoing medical procedures, the breast often deforms significantly. Accordingly, linear elasticity with the infinitesimal deformation formulation is not appropriate to formulate the FE model. As a result, we used a finite deformation formulation in conjunction with hyperelastic material. In a static condition, the equilibrium equation of a body under externally applied forces is

$$\frac{\partial \sigma_{i1}}{\partial x_1} + \frac{\partial \sigma_{i2}}{\partial x_2} + \frac{\partial \sigma_{i3}}{\partial x_3} + f_i = 0; \qquad i = 1, 2, 3 \tag{1}$$

where the σs denote the Cauchy (true) stress tensor components and f_i represents the body force. In the finite deformation formulation, the current position of a point $\mathbf{x}$ is obtained by adding the displacement $\mathbf{u}$ to the corresponding reference position of the same point $\mathbf{X}$, i.e.,

$$\mathbf{x} = \mathbf{X} + \mathbf{u}. \tag{2}$$

The stresses are related to displacements ($\mathbf{u}$) via a strain energy function U which is defined as a function of the strain invariants. These invariants are obtained based on the deformation gradient $\mathbf{F}$ as follows:

$$\mathbf{F} = \frac{\partial \mathbf{x}}{\partial \mathbf{X}}. \tag{3}$$

To separate the deviatoric and volumetric effects, $\overline{\mathbf{F}} = J^{-1/3}\mathbf{F}$ is defined, where $J = \det(\mathbf{F})$ is the third strain invariant which represents the total volume change at the point. Using $\overline{\mathbf{B}} = \overline{\mathbf{F}}.\overline{\mathbf{F}}^T$, the other strain invariants $\overline{I}_1$, $\overline{I}_2$ can be defined as follows:

$$\overline{I}_1 = \mathrm{tr}\left(\overline{\mathbf{B}}\right)$$
$$\overline{I}_2 = \tfrac{1}{2}\left(\overline{I}_1^2 - \mathrm{tr}\left(\overline{\mathbf{B}}.\overline{\mathbf{B}}\right)\right).$$

Assuming that a strain energy function $U = U(\overline{I}_1, \overline{I}_2, J)$ is selected, the true stress tensor can be obtained using the following equation [11]:

$$\sigma = \frac{2}{J}\left[\left(\frac{\partial U}{\partial \overline{I}_1} + \overline{I}_1 \frac{\partial U}{\partial \overline{I}_2}\right)\overline{\mathbf{B}} - \frac{\partial U}{\partial \overline{I}_2}\overline{\mathbf{B}}.\overline{\mathbf{B}}\right] + \frac{\partial U}{\partial J}\mathbf{I} \tag{4}$$

where $\mathbf{I}$ is the unit matrix. Considering the boundary conditions, (1) and (4) must be solved simultaneously to calculate the displacements $\mathbf{u}$. These equations are solved numerically through the FE method. In this method, after the domain is discretized into a number of homogeneous elements, a nonlinear system of equations is formed that is solved iteratively using Newton's method. This formulation is implemented in ABAQUS, a commercial FE software [11]. Discretization, i.e., mesh generation, especially in medical applications, is the most tedious step in a FE analysis. This step is described in the following sections.

B. Image Acquisition

We have developed meshing techniques which use MR images as an input to create FE meshes. In this work, two sets of MR images were acquired for a phantom and a volunteer's breast. The MR images were acquired using a GE SIGNA 1.5-T scanner (GE Medical Systems, Milwakee, WI). For the phantom, a 5.0-in surface coil was used to acquire T1-weighted axial images. A two-dimensional (2-D) spin-echo pulse sequence was used with 90° flip angle, TR/TE = 400.0/10.5 msec timing properties, 12 × 12 cm field of view (FOV), 256 × 128 resolution and 1.0-mm slice thickness. A magnitude image of this phantom is shown in Fig. 1, in which the inclusion can be seen with subtle contrast. For the breast, T1 weighted sagittal images were obtained using body coil. A 2-D spin-echo pulse sequence was used with 90° flip angle, TR/TE = 300.0/9.0 ms timing properties, 20 × 20 cm FOV, 256 × 128 resolution, 3.0-mm slice thickness, and three acquisitions.

C. Image Segmentation and Edge Detection

The purpose of segmentation is to separate different materials within the object of interest. This is done based on the MR signal intensity of different tissues. In the breast, the two main components, i.e., adipose and fibroglandular tissues, must be

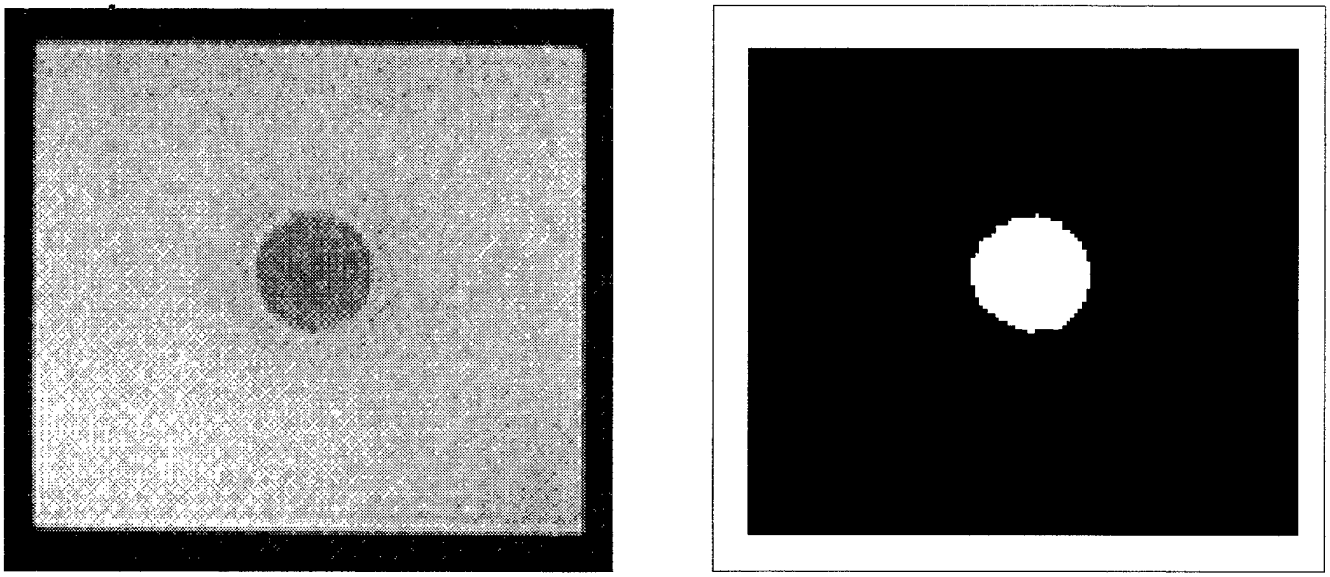

(a) (b)

Fig. 1. (a) A typical MR image and (b) a corresponding segmented image of the phantom.

segmented. For edge detection, as the breast tissues have significant signal intensity compared to the background with only noise signal, segmentation results in automatic breast edge detection. For segmentation, 3-D MRI data of the breast is converted into AnalyzeAVW 2.5 [24] database where a standard thresholding-based tool was used to yield segmented images that are suitable for FE mesh generation.

D. Voxel-Based (VB) Mesh Generation Technique

Because of the complex geometry of the breast and the structure of the fibroglandular tissue, common mesh generators require a significant amount of user interaction which is very time consuming. As an attempt to minimize user interaction throughout the mesh generation step, we have developed an automatic VB mesh generator with the aim of creating relatively accurate FE meshes of complex volumetric data efficiently. In fact, the only step which requires user interaction in this technique is the segmentation step. To construct the mesh, eight noded hexahedral elements are chosen. This type of element is well known to have many favorable characteristics over tetrahedral elements which can demonstrate overstiffening and locking behavior [12]. Right-angled hexahedrals, however, cannot model curved surface geometries which in turn leads to some inaccuracies in surface strains. To improve the mesh in this respect, we used the smoothing technique of Camacho *et al.* [25] which smooths irregular boundaries at model surfaces and material interfaces.

In the VB methods, since one FE is generated corresponding to each voxel, high resolution MR images may lead to huge FE meshes which, due to current computer power limitations, cannot be processed. Moreover, beyond a certain point, finer FE meshes do not practically improve the solution accuracy. Therefore, reducing image resolution is required to meet computational power constraints. For this purpose, a larger voxel size is selected and using the segmented images, the adipose and fibroglandular tissues voxels within each new voxel are counted. The new voxel will then be assigned to be as the one with the larger count.

After segmentation and resolution reduction, the mesh generation process is followed by node, and later element generation. For node generation, based on the pixel size, slice thickness and the coordinate system of the MR scanner, the nodes are arranged in the form of a 3-D rectangular lattice which confines the breast volume. The node coordinates of the lattice are calculated and placed in an array. Working with the regular lattice, later, facilitates element generation significantly because each neighbor node can be determined easily and accessed very quickly in the node array. The lattice, however, represents regions both inside and outside the breast. Regions outside the breast are determined during the element generation process and then discarded from the nodes array after element generation is done.

For element generation, the segmented image of each slice is loaded by the computer and stored in a 2-D array. To facilitate finding the boundary of each slice automatically, we assume that the fibroglandular tissue is surrounded by the adipose tissue portion. If this is not the case, a very thin one pixel size layer which represents adipose tissue can be added on the image manually using XV 3.10a image processor [26] to close the boundary where necessary. The boundary points are found by searching the image array line by line first from left to right and then from right to left until an adipose tissue pixel on the left and right boundaries is reached. These points are stored in two arrays that are later used in element generation. Elements corresponding to adipose and fibroglandular tissues are generated in each slice row by row starting from the left boundary point as the local first element node. Other nodes in each element are determined based on the local numbering scheme of hexahedral element. Element generation in a row is continued until the point prior to the right boundary point is reached. This process is repeated for each row to obtain a slice mesh and then for each slice to cover the entire breast. Slice meshes are then stacked to reconstruct a complete 3-D mesh. Skin elements are

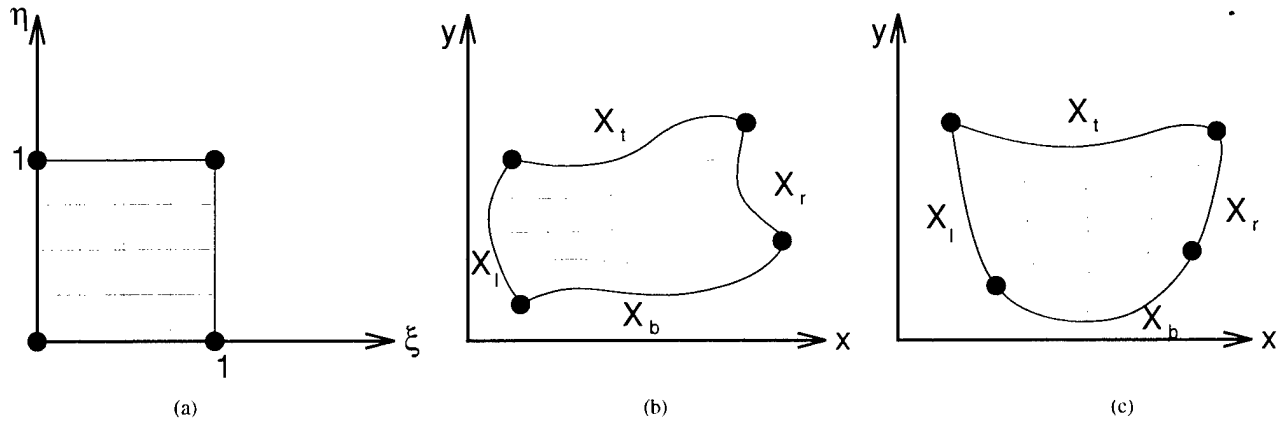

Fig. 2. (a) A unit square (logical space). (b) A typical physical space. (c) Breast boundaries in the TI meshing technique.

generated using four noded quadrilateral membrane elements. These elements are generated by identifying the outer face of elements on the breast surface. Finally, for smoothing, the node coordinates are modified using the smoothing technique of Camacho *et al.* [25]. In this technique, a smoothing coefficient which varies from zero for no smoothing to 0.5 for maximum smoothing, must be selected by the user. While higher factors result in smoother surfaces and interfaces, i.e., better geometry modeling, element distortion caused by this process leads to less accurate FE analysis. Therefore, to achieve optimal results, the smoothing coefficient must be selected or determined carefully. The meshing algorithm is implemented by creating a MATLAB program which inputs the segmented axial, coronal or sagittal images obtained from MRI data, generates the FE mesh, and outputs an input file compatible with ABAQUS FE software [11]. Henceforth, this meshing program will be referred to as VBMESH.

E. Transfinite Interpolation Mesh Generation Technique

This technique is based on the idea of mapping a unit square (logical space) to any given shape enclosed by four boundaries (physical space) [23]. To implement this idea in breast FE meshing, after image segmentation, the breast boundary in each slice is divided into three segments. Adding the boundary representing the chest wall, as shown in Fig. 2, the breast area will be enclosed by four boundaries. Although not necessary, these boundaries can be fitted by polynomials to smooth out the surface which is corrupted as a result of segmentation errors. After obtaining the breast boundaries in each slice image, the nodes are generated by mapping the nodes of the unit square grid to a set of nodes distributed inside the boundaries using the following equation:

$$\begin{aligned} X(\xi,\eta) = {} & (1-\eta)X_b(\xi) + \eta X_t(\xi) + (1-\xi)X_l(\eta) \\ & + \xi X_r(\eta) - \xi\eta X_t(1) - \xi(1-\eta)X_b(1) \\ & - \eta(1-\xi)X_t(0) - (1-\xi)(1-\eta)X_b(0) \end{aligned} \quad (5)$$

where ξ and η represent the unit square variables and X_b, X_t, X_l and X_r represent the breast's bottom, top, left and right boundaries respectively. Element connections determination in this technique is straight forward as it is done using the nodes of the unit square's grid. Using the same logic, the FE mesh of the skin is created by finding node connections of three of the unit square's circumferential lines corresponding to the breast's surface. After elements in each slice are generated, as in the previous method, they are stacked to construct a 3-D mesh.

Compared to the VB technique, this method requires a significantly smaller number of elements to represent the true geometry of the breast's surface. Furthermore, this method is capable of locally refining the mesh at an ROI by choosing smaller intervals in the corresponding logical space. Similar to VBMESH, this algorithm was implemented by a MATLAB program which will be, henceforth, referred to as TIMESH.

III. Results

A. Meshing Techniques Validation and Comparison

To validate the meshing techniques, the agarose phantom illustrated in Fig. 3 was constructed. This phantom consists of a block of agar (2%) with a hard cylindrical inclusion made of a mixture of 2% agar and 10% glass beads centered at (32.8, 30.5). The glass beads were used to enhance the contrast in the MR image for segmentation purposes. We assume that the Young's moduli of the block and the inclusion are respectively 11.0 Kpa and 55.0 Kpa. The block is also assumed to undergo a static loading due to 9.0-mm compression resulting from a laterally moving rigid plate toward another stationary plate as illustrated in Fig. 3. The phantom was scanned using a 5.0-in surface coil and a set of 60 MR images was acquired. These images were segmented and the resolution was reduced by a factor of four in the x and y directions and to 16 slices in the z direction. An MR image of the phantom and a corresponding segmented image are shown in Fig. 1. The obtained images were processed by VBMESH using a smoothing coefficient of 0.3 and a FE mesh was created. By dividing the inclusion's circumference into four segments and fitting each segment with a quadratic polynomial, another mesh was created using TIMESH. Finally, based on the known geometry of the phantom, a mesh was created manually as a bench mark. Corresponding to each mesh, an input file compatible with ABAQUS was created. These input files were preprocessed and their corresponding meshes are displayed in Fig. 4. Based on the nonlinear finite deformation FE formulation, the meshes were analyzed using ABAQUS 5.8.1, and as a result, the displacements, strains and stresses were calculated. It is well known that in FE analysis the most significant errors are encountered at material interfaces and curved surfaces which

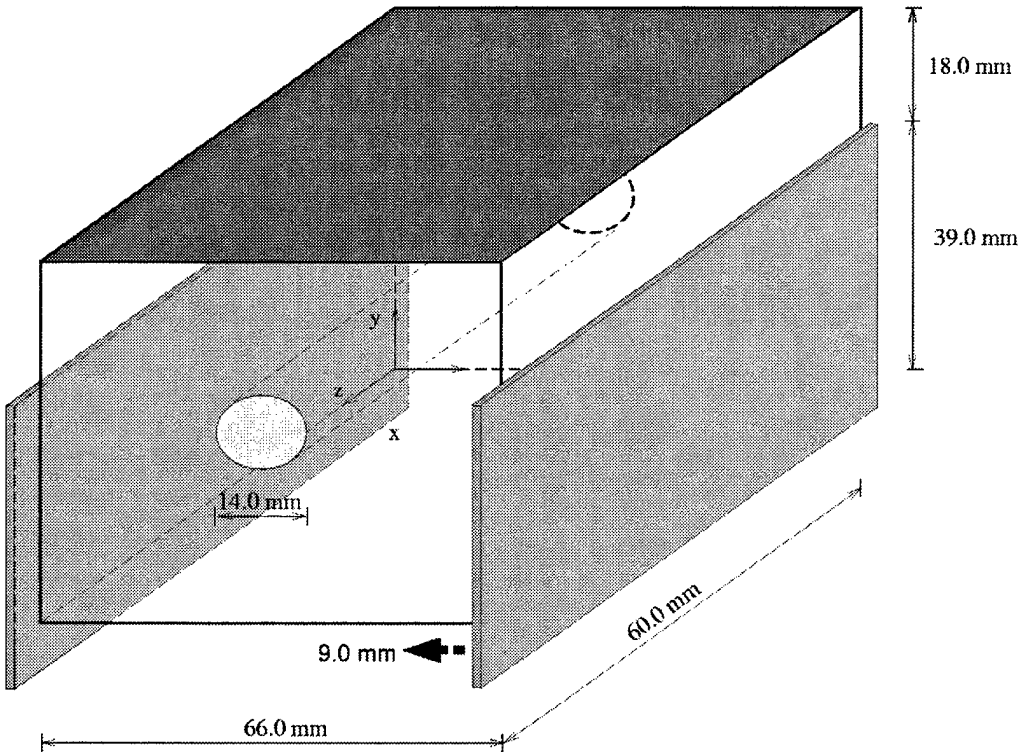

Fig. 3. A schematic of the phantom and its compression model.

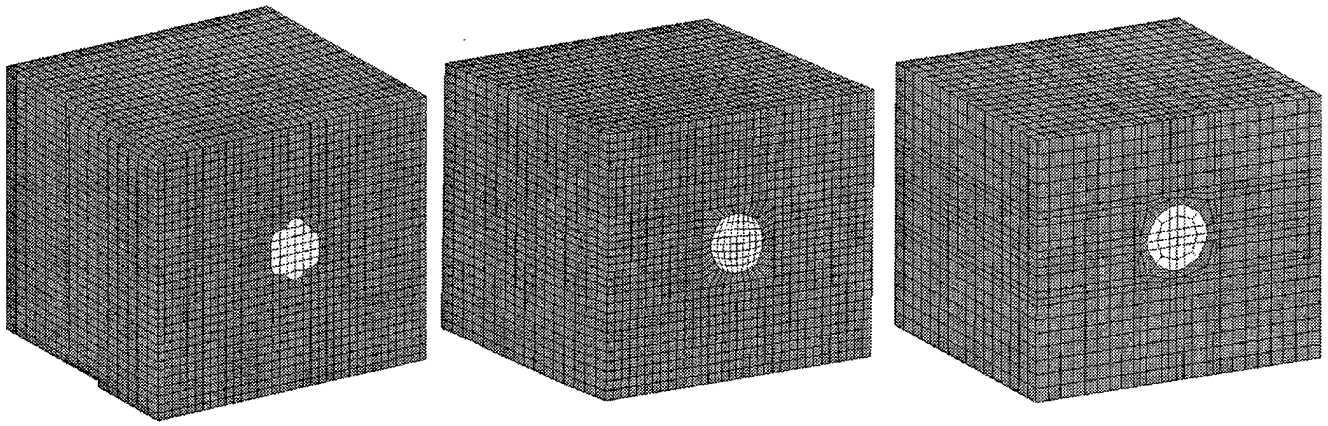

Fig. 4. (a) VB FE mesh, (b) TI-based FE mesh, and (c) A manually created FE mesh of the phantom.

are not represented appropriately by the FE mesh [22]. Therefore, to assess the accuracy of the presented meshing techniques, we will focus on the nodal values at the inclusion's circumference. As an example, the results of a displacement, a strain, and a stress component at this region in the middle plane are displayed in Fig. 5, which qualitatively indicates the better performance of the TI-based technique. To make a quantitative comparison, the average $\overline{E}$ and standard deviation σ of the relative error of the displacement, strain and stress over the inclusion's circumferential nodes are calculated and summarized in Table I. The results clearly indicate that the TI-based technique leads to more accurate FE meshes. Moreover, compared to the displacements errors, the strain and stress errors are significantly larger. This can be justified based on the fact that calculating both strains and stresses involves calculating the derivatives of displacements which leads to error magnification.

B. Breast Image Nonrigid Registration

To examine our model in a complex clinical problem, we applied it to a breast image registration problem where the breast was compressed by two plates causing nonrigid deformation. For this purpose, sagittal MR images of a breast of a healthy volunteer were acquired at 6-mm intervals at a resolution of 0.625 mm/pixel. These images were segmented with AnalyzeAVW 2.5 and the resulting images were processed to create FE meshes. A typical sagittal MR image of the breast and a corresponding segmented image are shown in Fig. 6(a) and (b). The objective here was to calculate MR images of

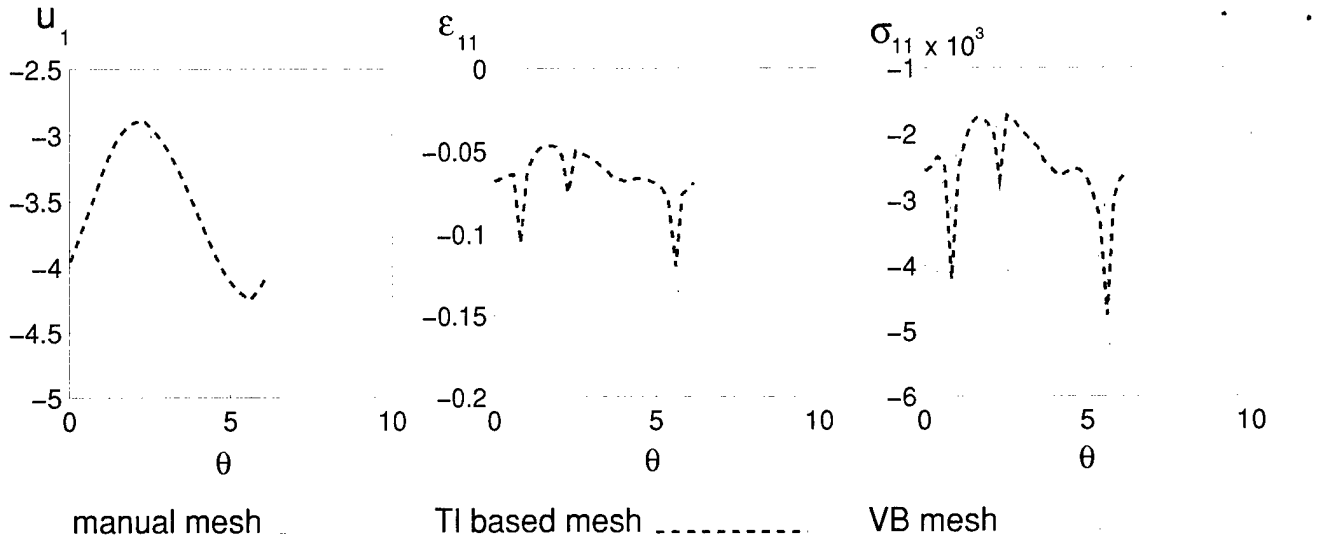

Fig. 5. Variations of the displacement, normal strain, and normal stress in the compression direction around the inclusion's circumference.

TABLE I
AVERAGE RELATIVE ERRORS $\bar{E}$ AND STANDARD DEVIATION σ OF DISPLACEMENTS, STRAINS, AND STRESSES OF THE CALCULATED MESHES AT THE INCLUSION'S SURFACE

Displacements	u_1	u_2	u_3	-	-	-
VB Mesh: $\bar{E}$ (%)	7.50	7.93	5.67	-	-	-
σ (%)	1.38	4.07	3.07	-	-	-
TI Mesh: $\bar{E}$ (%)	1.70	2.04	0.84	-	-	-
σ (%)	0.50	1.69	0.78	-	-	-
Strains	ϵ_{11}	ϵ_{22}	ϵ_{33}	ϵ_{12}	ϵ_{13}	ϵ_{23}
VB Mesh: $\bar{E}$ (%)	18.14	16.94	6.32	16.56	20.86	20.89
σ (%)	7.00	9.79	4.79	11.00	15.23	20.91
TI Mesh: $\bar{E}$ (%)	14.24	8.08	9.82	17.89	13.10	16.33
σ (%)	11.25	7.17	2.83	12.83	10.21	17.27
Stresses	σ_{11}	σ_{22}	σ_{33}	σ_{12}	σ_{13}	σ_{23}
VB Mesh: $\bar{E}$ (%)	17.15	14.55	9.37	16.56	20.86	20.89
σ (%)	9.32	14.89	10.32	11.00	15.23	20.91
TI Mesh: $\bar{E}$ (%)	13.20	8.21	12.03	17.89	13.10	16.33
σ (%)	10.70	8.31	5.36	12.83	10.21	17.27

this breast as if it underwent 8.0-mm compression. For this purpose, two FE meshes were first created using the VB and TI-based techniques. After image segmentation and resolution reduction by a factor of 4 in each direction, the resulting images were processed by VBMESH using a smoothing coefficient of 0.3. The resulting mesh consists of 16 841 elements and 15 939 nodes and is characterized by an abrupt surface. Using the segmented images, the TI-based mesh was created using TIMESH. This mesh was calculated by fitting a third-order polynomial to the boundary representing the chest wall while fitting quadratic polynomials to the breast surface's three segments. The resulting mesh consists of 2280 elements and 2059 nodes and, unlike the VB mesh, has a smooth surface. The FE meshes of one slice created using the VB and the TI-based techniques are depicted in Fig. 6(c) and (d). Fig. 7 depicts the VB mesh, the TI-based mesh of the entire breast, and the breast FE model undergoing compression. The adipose and fibroglandular tissues were assumed to be incompressible and hyperelastic, and the corresponding parameters were obtained by fitting experimental data [9] to a hyperelastic Neo–Hookean model. For this purpose, the data represented as Young's modulus versus strain were converted to stress versus strain by first fitting quadratic and third-order polynomials to the adipose and fibroglandular tissues data, respectively, then integrating over the strain. The resulting fitting polynomials of the Young's modulus versus strain of the adipose and fibroglandular tissues are as follows:

$$E = 0.5197\epsilon^2 + 0.0024\epsilon + 0.0049; \quad \text{for fat}$$

$$E = 123.8889\epsilon^3 - 11.7667\epsilon^2 + 0.6969\epsilon + 0.0121; \quad \text{for parenchyma.}$$

To the authors' knowledge, the experimental data [9] are the only available breast tissue hyperelastic properties data obtained based on the large deformation theory considerations. Nevertheless, as the standard deviation of this data is high, more accurate and reliable data is required to produce better image registration results. Skin, in general, is well known to be anisotropic and hyperelastic [27]. However, it can be approximated by an isotropic and linear elastic model provided that the strain does not exceed 50% [27], [28]. Accordingly, as the skin strain in this application is expected to be well below 50%, it was assumed to be elastic with a Young's modulus of 10.0 kPa [28] and a thickness of 1.0 mm. The chest wall was assumed to provide zero displacement boundary conditions while the specified displacement or force boundary conditions on the breast's surface is not known because the contact surface between the breast and the plates increases over the course of compression. Accordingly, this problem was formulated as a 3-D contact problem and ABAQUS' contact solver with the finite deformation theory formulation was used. This highly nonlinear problem was solved iteratively and, as a result, the breast tissue displacements were calculated. These displacements, in combination with the MR images of the uncompressed breast, were used to obtain simulated MR images of the compressed breast. A number of consecutive sagittal MR images of the breast before compression, along with their corresponding simulated images after compression, are depicted in Fig. 8. In this figure, reasonable translation and tissue expansion can be observed by comparing the two sets of images. For example, image (g′) from the simulated set and

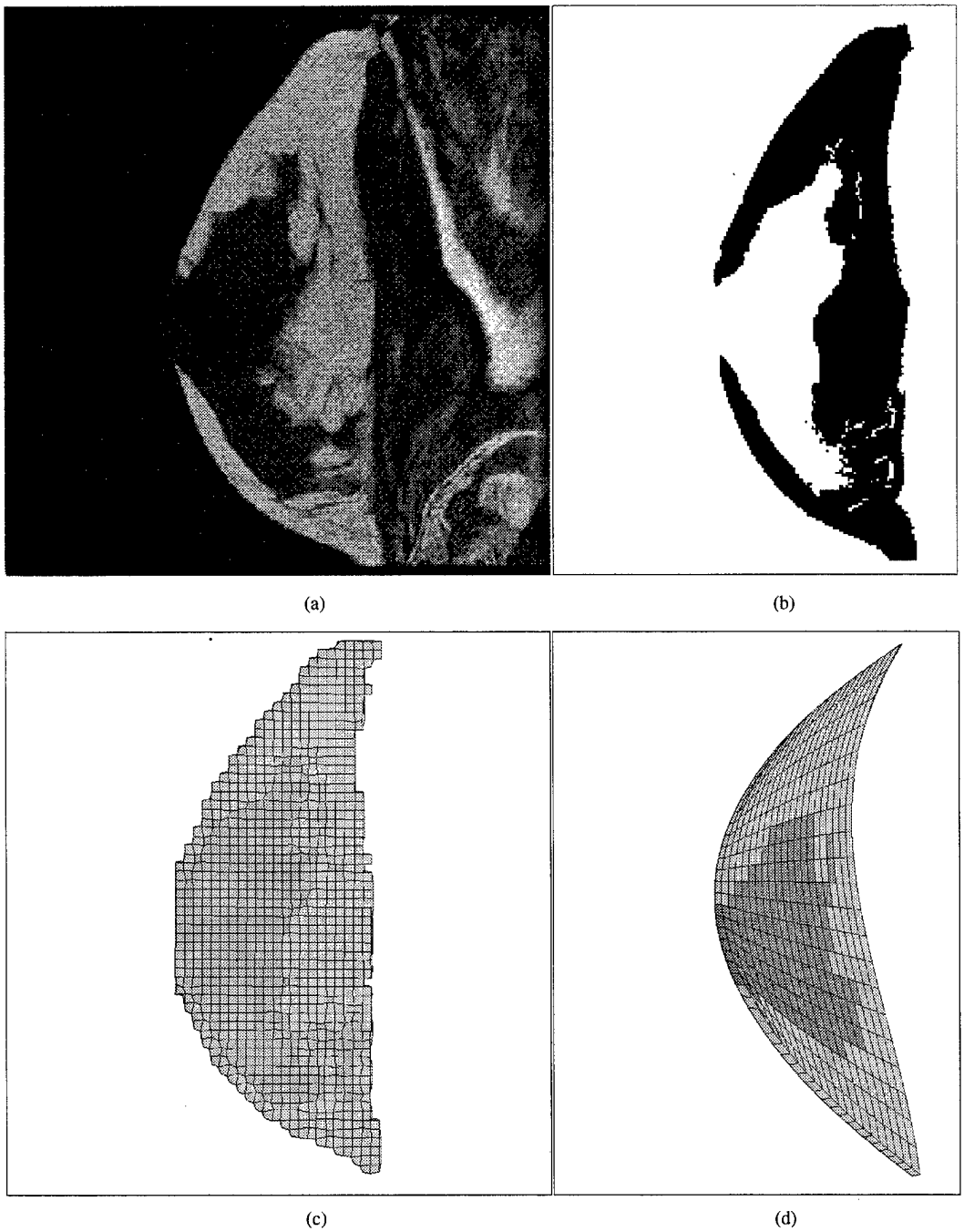

Fig. 6. (a) A MR image and (b) a corresponding segmented image, (c) VB FE mesh, and (d) TI-based FE mesh of one breast slice.

image (f) from the MR image set, which approximately correspond to the same slice, depict similar anatomical features. The same can be observed in other image pairs such as (a, b'), (b, c'), etc.

IV. Discussion

We have presented a FE model, based on biomechanical principles, to predict breast tissue deformations. This model can serve as a guideline in numerous clinical applications, such as breast image registration, multimodality data fusion, breast surgery, and biopsy. The first component of this model is FE meshing, for which two meshing techniques were presented and evaluated. These techniques, which require minimal user interaction, use MRI images of the breast to produce patient-specific FE meshes. Using a numerical experiment, the TI-based meshing technique, which requires fewer elements to represent the geometry of curved surfaces relatively accurately, proved to generate more accurate displacements and stresses. Moreover, unlike the VB technique, this technique is capable of refining the mesh at an arbitrary ROI. The adipose and fibroglandular tissues are modeled as incompressible and hyperelastic materials while the skin is modeled using membrane elements with linear elastic properties. These tissues are assumed to

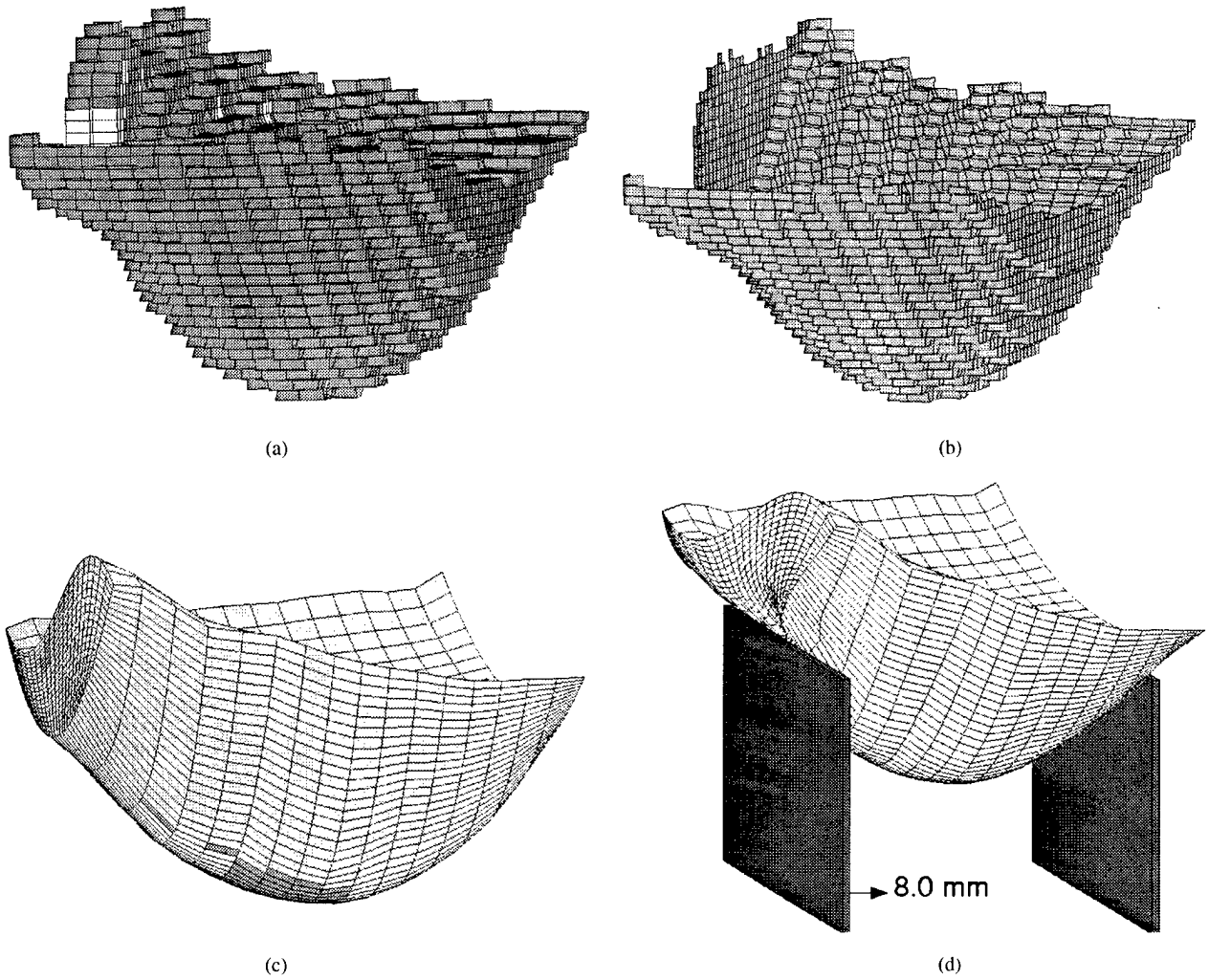

Fig. 7. (a) VB 3-D FE mesh of the breast slice excluding the skin, (b) corresponding skin mesh, (c) TI-based FE mesh of the breast, and (d) the deformed shape of the breast under compression.

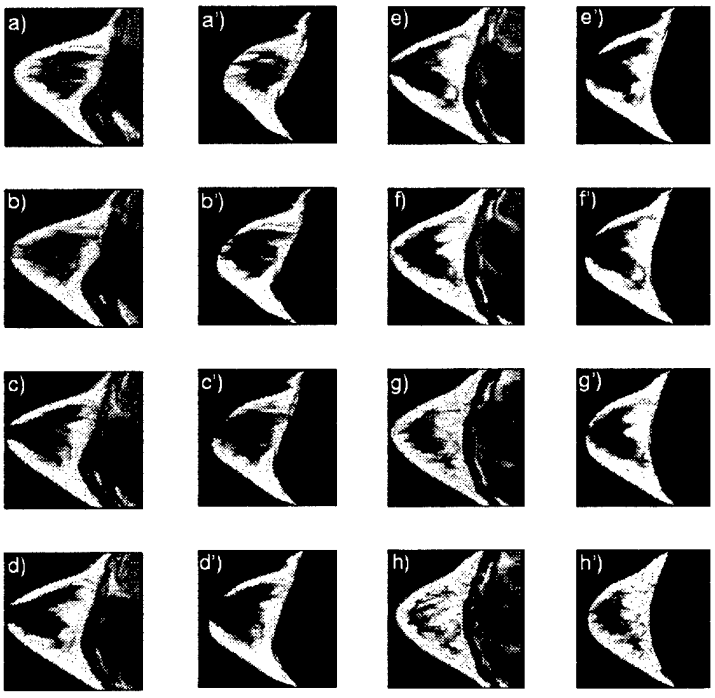

Fig. 8. MR images of the breast before compression (a, b, c, etc.) and simulated images of the compressed breast (a', b', c', etc.).

undergo large deformations. As for boundary conditions, the chest wall region is assumed to provide zero displacements boundary conditions while the specified boundary conditions depend on the clinical application. For example, in the breast image registration problem, as was previously presented, this boundary condition type is not known explicitly and the problem is formulated as a 3-D contact problem. An image registration example was presented to evaluate the FE model's effectiveness in complex clinical applications. The results summarized in Fig. 8 qualitatively prove the merits of this model. Quantitative validation, however, is beyond the scope of this paper as it requires more reliable breast tissue hyperelastic properties data. Research is underway in our laboratory to acquire such data which will pave the way for conducting this validation.

REFERENCES

[1] A. Samani, J. Bishop, E. Ramsay, and D. Plewes, "Breast tissue deformation finite element modeling for MRI/X-ray mammography data fusion," presented at the 5th Int. Workshop Digital Mammography, Toronto, ON, Canada, 2000.

[2] J. H. Keyak, J. M. Meagher, H. B. Skinner, and C. D. Mote, "Automated three-dimensional finite element modeling of bone: A new method," *J. Biomed. Eng.*, vol. 12, pp. 389–397, 1990.

[3] R. Müller and P. Rüegsegger, "Three-dimensional finite element modeling of noninvasively assessed trabecular bone structure," *Med. Eng. Phys.*, vol. 17, no. 2, pp. 126–133, 1995.

[4] W. Krach, T. J. Rammerstorfer, T. J. Reiter, and P. Zenz, "*In vivo* CT-based 3-D-modeling of human bones with respect to inhomogeneity," in *Proc. ASME Bioengineering Conf.*, vol. BED-29, 1995, pp. 57–58.

[5] J. M. Guccione, K. D. Costa, and A. D. McCulloch, "Finite element stress analysis of left ventricular mechanics in the beating dog heart," *J. Biomech.*, vol. 28, pp. 1167–1177, 1995.

[6] S. K. Kyriacou, C. Davatzikos, S. J. Zinreich, and R. N. Bryan, "Nonlinear elastic registration of brain images with tumor pathology using a biomechanical model," *IEEE Trans. Med. Imag.*, vol. 18, pp. 580–592, July 1999.

[7] M. I. Miga, J. M., K. D. Paulsen, Lemery, S. D. Eisner, A. Hartov, F. E. Kennedy, and W. R. D., "Model-updated image guidance: Initial clinical experiences with gravity-induced brain deformation," *IEEE Trans. Med. Imag.*, vol. 18, pp. 866–874, Oct. 1999.

[8] A. Hagemann, K. Rohr, H. S. Stiehl, U. Spetzger, and J. M. Gilsbach, "Biomechanical modeling of the human head for physically based nonrigid image registration," *IEEE Trans. Med. Imag.*, vol. 18, pp. 875–884, Oct. 1999.

[9] P. S. Wellman, "Tactile imaging," Ph.D. dissertation, Harvard Univ., Cambridge, MA, 1999.

[10] J. M. Sullivan Jr., G. Charron, and K. D. Paulsen, "A three-dimensional mesh generator for arbitrary multiple material domain," *Finite Elements Anal. Design*, vol. 25, pp. 219–241, 1997.

[11] *ABAQUS, Theory Manual*, Hibbit, Karlsson, and Sorenson, Pawtucket, RI, June 1998.

[12] T. J. R. Hughes, *The Finite Element Method, Linear Static and Dynamic Finite Element Analysis*. Englewood Cliffs, NJ: Prentice-Hall, 1987.

[13] R. T. Hart, V. V. Hennebel, N. Thongpreda, W. C. Van Buskirk, and R. C. Anderson, "Modeling the biomechanics of the mandible: A three-dimensional finite elemeny study," *J. Biomech.*, vol. 25, pp. 261–286, 1992.

[14] M. J. Rudert and T. D. Brown, "Toward automation of finite element models for bone grafting of femoral head osteonecrosis," in *Proc. ASME Bioengineering Conf.*, vol. BED-28, 1994, pp. 145–146.

[15] V. K. Goel, H. Park, and W. Kong, "Investigation of vibration characteristics of the ligamentous spine using the finite element approach," *J. Biomech. Eng.*, vol. 116, pp. 377–383, 1994.

[16] E. H. II Moor, D. A. Schauer, and J. A. Weiss, "Mesh generation for a finite element model of the human leg," in *Proc. ASME Bioengineering Conf.*, vol. BED-29, 1995, pp. 51–52.

[17] L. Voo, J. A. Denman, N. Yoganandan, and F. Pintar, "A 3-D model of the cervical spine with ct-based geometry," *Adv. Bioeng.*, vol. 29, pp. 323–324, 1995.

[18] D. P. Fyhrie, M. S. Hamid, R. F. Kuo, and S. M. Lang, "Direct three-dimensional finite element analysis of human vertebral cancelous bone," in *Proc. 38th Annu. Meeting Orthopedic Research Society*, vol. 17, 1992, p. 551.

[19] S. J. Hollister and N. Kikuchi, "Direct analysis of trabecular bone stiffness and tissue level mechanics using an element by element homogenization method," in *Proc. 38th Annu. Meeting Orthopedic Research Society*, vol. 17, 1992, p. 559.

[20] B. van Rietbergen, H. Weinans, R. Huiskes, and A. Odgaard, "A new method to determine trabecular bone elastic properties and loading using micromechanical finite-element models," *J. Biomech.*, vol. 28, pp. 69–81, 1995.

[21] C. R. Jacobs, J. A. Mandell, and G. S. Beaupre, "A comparative study of automatic finite element mesh generation techniques in orthopedic biomechanics," in *Proc. ASME Bioengineering Conf.*, vol. BED-24, 1993, pp. 512–514.

[22] R. E. Guldberg and S. J. Hollister, "The accuracy of digital image-based finite element models," *J. Biomech. Eng.*, vol. 120, no. 2, pp. 289–295, 1998.

[23] P. Knupp and S. Steinberg, *Fundamentals of Grid Generation*. Boca Raton, FL: CRC, 1994.

[24] "AnalyzeAVW, Ver. 2.5," Mayo-Foundation, Rochester, MN, 1998.

[25] D. L. A. Camacho, R. H. Hopper, G. M. Lin, and B. S. Myers, "An improved method for finite element mesh generation of geometrically complex structures with application to the skullbase," *Biomechanics*, vol. 30, no. 10, pp. 1067–1070, 1997.

[26] *XV. Ver. 3.10a*, J. Bradley, 1994.

[27] P. Tong and Y. C. Fung, "The stress-strain relationship for the skin," *J. Biomechanics*, vol. 9, pp. 649–657, 1976.

[28] J. E. Bischoff, E. M. Arruda, and K. Grosh, "Finite element modeling of human skin using an isotropic, nonlinear elastic constiutive model," *J. Biomech.*, vol. 33, pp. 645–652, 2000.